Research in Astronomy and Astrophysics, 22:115001 (7pp), 2022 November https://doi.org/10.1088/1674-4527/ac71fc

Evidence of Quasi-periodic Oscillation in the Optical Band of the Blazar 1ES 1959+650

Fu-Tong Dong[1,2], Ning Gai[1], Yanke Tang[1], Yi-Fan Wang[1], and Ting-Feng Yi[3]
[1] College of Physics and Electronic Information, Dezhou University, Dezhou 253023, China; dongfutong@sohu.com
[2] Technological Vocational College of Dezhou, Dezhou 251200, China
[3] Key Laboratory of Colleges and Universities in Yunnan Province for High-energy Astrophysics, Department of Physics, Yunnan Normal University, Kunming 650500, China
Received 2022 March 8; revised 2022 April 22; accepted 2022 May 16; published 2022 October 12

Abstract

We analyzed the optical monitoring data in the *R* band of TeV blazar 1ES 1959+650 from 2002 to 2018, and provided evidence of a quasi-periodic oscillation in this object. The light curve shows a stable and persistent periodicity at ∼540 days, detected by the Lomb–Scargle periodogram, Jurkevich and weighted wavelet z-transform techniques. The red noise power spectrum was estimated using the PSRESP method, and this period was found to be at $>3\sigma$ significance level. There are also two possible periodicities at ∼268 and ∼1100 days detected by all three methods. However, their significance levels are relatively low, and thus these two periods cannot be verified by the present data. We discuss several possible physical models that could explain the periodic variability in this object.

Key words: galaxies: active – methods: numerical – galaxies: individual (1ES 1959+650)

1. Introduction

Blazars are a subgroup of active galactic nuclei (AGNs), typically showing violent variability at almost all wave bands with strongly polarized emission (Urry & Padovani 1995). Most of their non-thermal emissions are thought to come from a relativistic jet lying close to our line of sight (Krawczynski 2004; Böttcher 2007; Abdo et al. 2010). Generally, there are two broad bumps in the spectral energy distributions (SEDs) of blazars: the first bump (synchrotron peak) is in the radio to X-ray band and the second one peaks in the gamma-ray band (Böttcher 2007; Finke et al. 2008; Reynoso et al. 2011; Anjum et al. 2020). According to the synchrotron peak frequency ν_s, blazars can be classified into three subgroups: low synchrotron peaked (LSP) with $\nu_s \leqslant 10^{14}$ Hz, intermediate synchrotron peaked (ISP) with 10^{14} Hz $< \nu_s < 10^{15}$ Hz and high synchrotron peaked (HSP) with $\nu_s \geqslant 10^{15}$ Hz (Abdo et al. 2010).

Blazar variability can be divided into three classes based on different timescales: intra-day variability (IDV) or microvariability which has timescales of minutes or hours, short-term variability (STV) with timescales ranging from one day to months, and long-term variability (LTV) with timescales of the order of years (Fan 2005; Fan et al. 2007; Gupta et al. 2016). A commonly detected feature of blazar variability is quasi-periodic oscillations (QPOs) (Sandrinelli et al. 2016). These phenomena have been observed in multi-wavelength (including gamma-ray, X-ray, optical and radio) light curves, with timescales ranging from minutes to years. Detections of QPOs on intra-day timescale are relatively rare. In the past decades, only several blazars have been reported to have QPOs on this timescale, e.g., Espaillat et al. (2008) claimed a ∼55 minute QPO in the X-ray light curve of 3C 273; Rani et al. (2010) reported a significant QPO of ∼15 minutes in the optical band of s5 0716+714. Long-term or short-term QPOs, on the other hand, are routinely detected (e.g., Wang et al. 2014 for 1156 +295, Bhatta et al. 2016 for OJ 287, Ren et al. 2021 for PKS J0805-0111, etc.).

Searching for QPOs is an important tool in blazar variability studies. Several models or mechanisms have been proposed to describe the QPOs, such as the helical jet model (Caproni et al. 2013); the jet precession mechanism (Kudryavtseva et al. 2011; Beaklini & Abraham 2014); variations in accretion process (An et al. 2013), etc. Confirmed periodicities would help us assess the possible physical models and probe the physical properties of blazars.

In this paper, we analyze the LTV of the TeV blazar 1ES 1959+650 ($z = 0.048$; Perlman et al. 1996). The synchrotron peak of this source appears at ultraviolet to X-ray frequencies (Giebels et al. 2002), which makes it an HSP blazar. The source shows variability in different spectral bands. In gamma-ray bands, several "orphan" TeV flares have been detected (Krawczynski et al. 2004; Böttcher 2005; Kapanadze et al. 2016) . In X-rays, the source displays rapid variability with fractional amplitudes of 5.4%–7.5% within 1 ks (Kapanadze et al. 2016, 2018). In optical, significant STVs and LTVs were detected (Kurtanidze et al. 2009; Gaur et al. 2012; Sorcia et al. 2013; Zhang & Li 2017). Yuan et al. (2015) observed IDVs in

the V, R and I bands on two nights in 2009. These authors also analyzed the long-term optical light curve and no quasi-periodicity was found. Similarly, Nilsson et al. (2018) searched QPOs of 31 TeV blazars including 1ES 1959+650 using data observed by the Tuorla/KVA telescope, and no evidence of periodic variation was found in their data set. In radio bands, Li et al. (2017) searched for QPOs in the 15 GHz light curve using data from the Owens Valley Radio Observatory (OVRO) 40 m telescope, but no statistically significant periodicity was found. In this work we re-analyzed the optical variability of 1ES 1959 +650 using data with longer time coverage, more data points and better time sampling, and found evidence of QPOs in this object.

2. Observational Data

We collected the optical R band photometric data for analysis of the variability of 1ES 1959+650 from several publicly available sources. Yuan et al. (2015) observed 1ES 1959+650 using the 1.56 m telescope at Shanghai Astronomical Observatory. Their data span a timescale of 8 yr from 2006 to 2014 with 153 data points. Zhang & Li (2017) reported their observational results using the 80 cm optical telescope at Xinglong Observatory; 149 data points were obtained from their observation spanning 2010 to 2016. Nilsson et al. (2018) published their R band data of 31 blazars from the Tuorla Blazar Monitoring Program, and the monitoring data of 1ES 1959+650 were obtained with 734 data points and a time coverage of 10 yr (2002–2012). Moreover, we obtained the R band observations reported by Sorcia et al. (2013). We also used the R band observations from the Small and Moderate Aperture Research Telescope System (SMARTS) (Bonning et al. 2012).

Finally, we obtained data observed by the 60/90 cm Schmidt telescope at Xinglong Observatory (Meng et al. 2018). These observations were performed in five filters, c, e, i, m and o. The central wavelength of the i band is close to that of the R band (Meng et al. 2018). Thus we transformed these data into the R band using the equation $R = 0.897 \times i + 1.127$ (Dai et al. 2013). However, the transformed magnitudes have large differences with the other data collected here. To match with the other observations, we subtracted 0.51 mag from the transformed data. This value was obtained by averaging the magnitude differences between the transformed data and the other data with observed time difference less than 15 minutes. The process was performed based on the assumption that there is no significant variability in such a short time interval, which is most probably true according to previous optical monitoring of this object.

Figure 1 depicts the optical R band light curve spanning 15.6 yr from September 2002 to June 2018 with a total of 1642 data points. The average sampling interval is ∼3.5 days, and the largest interval is ∼292 days. The colors signify data from different sources. The source shows irregular variability with three prominent outbursts signified by solid lines in the figure, corresponding to Julian Dates (JDs) ∼2453934, 2455036 and 2456053, which indicate an outburst time interval of ∼1000 days. There are also some accompanying small peaks showing ∼500 day time interval from the main peaks. Small amplitude IDVs are superposed on the LTVs.

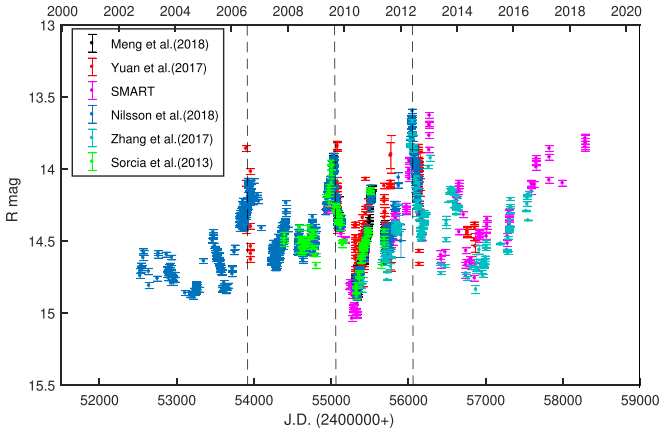

Figure 1. Optical light curve of 1ES 1959+650 in the R band. Different colors signify data from different observations.

3. Periodicity Analysis

In order to identify possible QPOs, we used three specialized techniques, the Lomb–Scargle (LS) periodogram, the Jurkevich method and the weighted wavelet z-transform (WWZ) to analyze the variability of 1ES 1959+650 and presented the results here. These techniques have different approaches in data analysis. This ensures the reliability of any detected QPOs in the data.

3.1. Lomb–Scargle Periodogram

The LS periodogram is a widely utilized technique in periodicity studies. This method is quite useful for unevenly sampled time series. It relies on a linear combination of sine and cosine functions to fit the data with a least-squares analysis (Lomb 1976; Scargle 1982; VanderPlas 2018). The method effectively reduces the spurious artificial peaks that are usually present in a classical periodogram when dealing with irregularly sampled data. The LS periodogram identifies periods as peaks in the periodogram. Figure 2 shows the LS periodogram of the observed data in the R band. To search for long-term QPOs in the light curve, we set the frequency range in 0.0005–0.01 day^{-1} in our calculations. The lowest frequency boundary ensures there are at least ∼3 repeating cycles in the observed data for any detected QPOs. Three prominent peaks appear in the periodogram, corresponding to periods of

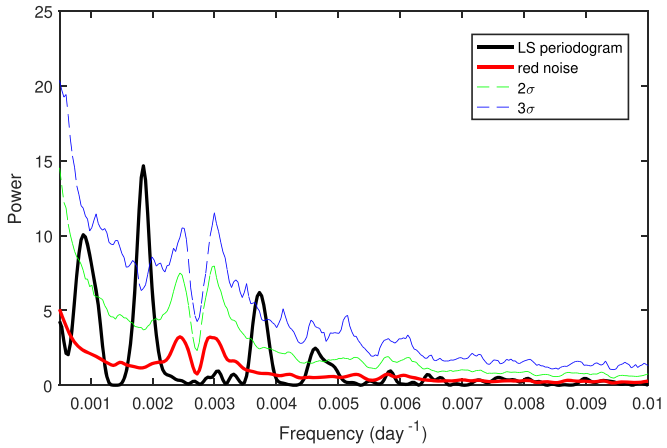

Figure 2. The LS power spectrum of the optical R band data of 1ES 1959 +650. The periodogram is marked in a black solid line. The red solid line, and the green and blue dashed lines correspond to the best-fit red noise power spectrum, and the curves of 2σ and 3σ confidence levels respectively.

$P_1 = 1134$ days, $P_2 = 540$ days and $P_3 = 268$ days respectively.

However, blazar power spectra are generally dominated by red noise, which appears as a steep power-law in the frequency domain and random, aperiodic variations in the time domain, and can act as quasi-periodic variations in a few cycles of the observed data, especially in the low-frequency domain (Timmer & Koenig 1995; Vaughan 2005; Vaughan et al. 2016). Thus it is important to include the impact of red noise processes in identifying periods in blazars. First, we employed the power spectrum response (PSRESP) method (Uttley et al. 2002) to model the red noise shape in the power spectrum of 1ES 1959+650. The method fits the binned power spectrum of the observed data with a given model shape using Monte-Carlo simulations. Here we modeled the source power spectrum using a power-law shape $P(\nu) \propto \nu^{-\alpha}$ with the slope α spanning the range of 1–2.5. We then generated 1000 simulated light curves with the same sampling, mean and uncertainties as the observed light curve for each trial value of α using the technique of Timmer & Koenig (1995). The power spectra of the simulated light curves were then averaged to get the mean profile of the model. This process was repeated for different values of alpha and each resulting mean shape was compared with that of the observed one to get the best-fit profile of the power spectral model. The effect of Poisson noise was also included in the calculations. The resulting best-fit model is displayed in Figure 2 (the red solid line) with the slope $\alpha = 1.7 \pm 0.2$.

In order to evaluate the effect of the red noise on the LS candidate periodicities shown above, we then simulated 10,000 light curves using the best-fit power spectrum to construct the 2σ (95%) and 3σ (99.73%) curves of confidence levels for the peaks in the periodogram. The result is shown in Figure 2. The power spectrum of each simulated light curve is generated using the LS periodogram and compared in each frequency with the observed power spectrum. This procedure is based on the null hypothesis that the variations in the observed light curve are simply due to red noise. As featured in Figure 2, the significance of the peaks at P_2 and P_3 turns out to be $>3\sigma$. This implies that these two periods are unlikely to be generated by the red noise processes. On the other hand, the peak at P_1 only has a confidence level of $>2\sigma$. Thus, we finally obtained two confident periodicities of 540 ± 38 and 268 ± 11 days. The uncertainties are estimated by fitting a Gaussian line to the peak after subtracting the best-fit power-law in the periodogram, as done in Bhatta et al. (2016).

3.2. Jurkevich Method

As a comparison, we also performed an analysis of the R band light curve of 1ES1959+650 using the Jurkevich method (Jurkevich 1971). This method is one of the phase folding techniques, and is more effective in processing non-sinusoidal modulated data than Fourier transform. The method is also suited for sparse and unequally sampled data, and has been widely applied in blazar QPO analysis. It bins the tested data according to different trial periods. With a given period, all data are assigned to a certain number of groups based on their phases. Then the variance V_i^2 of each group and the sums V_m^2 of all groups are calculated. V_m^2 reaches its minimum if a trial period is a genuine one, while it remains almost constant for a false trial period. Thus a much reduced minimum indicates a good period in the signal. However, practically V_m^2 is affected by various factors, such as the number of groups (m), the sampling of the data, etc. This will produce numerous spurious minima of V_m^2. Kidger et al. (1992) proposed that the fractional reduction of the variance based on the F-test could be a good test of the significance of a minimum (Fan et al. 1997; Xie et al. 2008),

$$f = \frac{1 - V_m^2}{V_m^2}, \tag{1}$$

where V_m^2 is the normalized variance. Normally, a value of $f \geqslant 0.5$ suggests a robust period in the data, while $f < 0.25$ indicates the period is weak.

Figure 3 shows the Jurkevich results of our calculations. The calculations were performed with $m = 10$. A minimum of $V_m^2 = 0.82$ is at the period 265 ± 10 days with $f = 0.2$, indicating the period is very weak or it is just a random process. The uncertainties in the periodicity are estimated by full width at half maximum (FWHM) of the minimum. An obvious minimum of $V_m^2 = 0.53$ with $f = 0.88$ is at the trial period of 540 ± 35 days, suggesting it is a strong periodicity. There is also a wide and deep valley with a minimum of $V_m^2 = 0.46$ at 1100 ± 120 days in the plot. The f value of the minimum is 1.16, implying it is a very strong period.

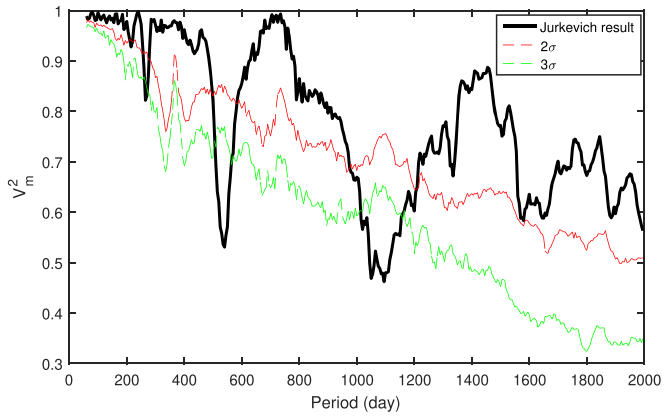

Figure 3. The Jurkevich result of the optical data of 1ES 1959+650. The red and green dashed lines trace the curves of 2σ and 3σ confidence levels respectively.

We also estimated the effect of red noise on the Jurkevich results using the method described in Section 3.1. The 2σ and 3σ confidence levels were constructed using 10,000 simulated light curves considering the best-fit power spectrum. As affirmed in Figure 3, the periodicity of 540 ± 35 days is well above the 3σ confidence levels, showing a very good agreement with P_2 detected in the LS periodogram. Meanwhile, the weak periodicity of 265 ± 10 days is also above the 3σ confidence levels, similar to P_3 detected in the LS periodogram. However, the period of 1100 ± 120 days also displays a significance level of $>3\sigma$, which is different from the result of the LS periodogram. This may be due to the periodic variation being non-sinusoidal, and the LS periodogram being inefficient to deal with this pattern of variations. However, we cannot confirm this periodicity based on the present data set. As suggested in Xie et al. (2008), to detect a reliable periodicity, the duration of the data sample must be at least six times the period. Thus more observations are needed to support the availability of the period.

3.3. Weighted Wavelet z-transform

Although the above two methods are powerful in analyzing irregularly sampled data set, they cannot specify the time fluctuations of the possible periodic signals. Actually, QPOs in astronomical data may vary both in their periods and amplitudes. Thus, in order to find out the physical processes causing the QPOs, it is important to identify their time evolutions. This can be done by wavelet transform. However, the method is only applicable to an evenly sampled data set, and may result in spurious time evolution for uneven time sampling. In this context, a more suitable form of the wavelet transform for unevenly spaced data set is the WWZ (Foster 1996). The technique modifies the wavelet transform as a weighted projection onto three trial functions $\phi_1(t) = 1(t)$, $\phi_2(t) = \cos(\omega(t-\tau))$, $\phi_2(t) = \sin(\omega(t-\tau))$ with the

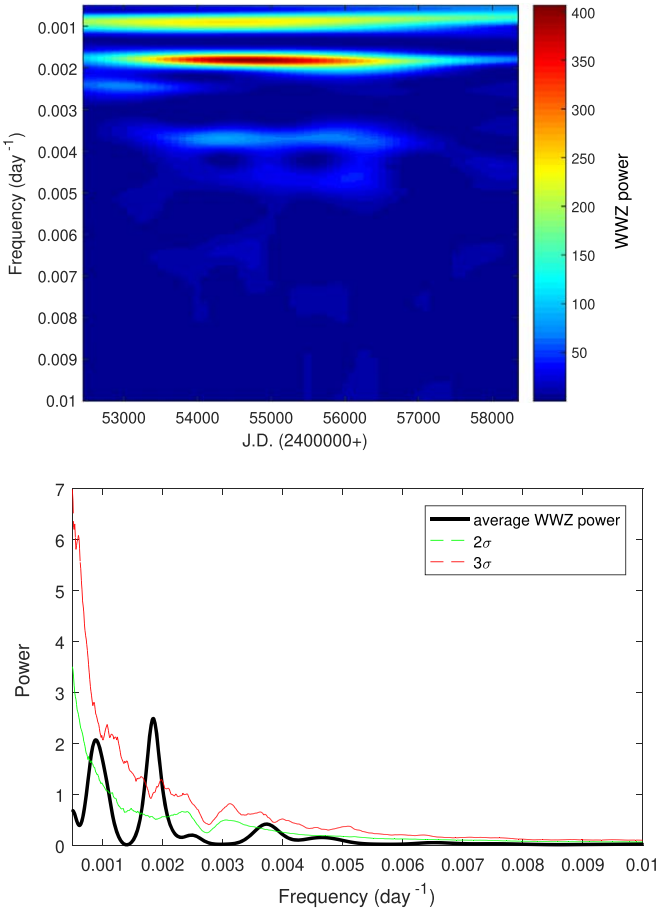

Figure 4. The WWZ analysis results of the optical data of 1ES 1959+650. (Top) The WWZ power as a function of time and frequency. (Bottom) The time averaged WWZ power spectrum together with the 2σ and 3σ confidence levels.

statistical weights $w_a = e^{-c(\omega(t-\tau))}$. The resulting WWZ power is in the form,

$$Z = \frac{(N_{\rm eff} - 3)V_y}{2(V_x - V_y)}. \quad (2)$$

Here V_x and V_y are the weighted variations of the data and the model function respectively, and $N_{\rm eff}$ is the effective number of data points (Foster 1996).

The WWZ power of the R band magnitude of 1ES 1959 +650 is displayed in the upper panel of Figure 4. The frequency was set in the range of 0.0005–0.01 day^{-1}, as in the LS periodogram calculations. Two persistent periodic signals (which appear as continuous features over the whole observed time range) are distinctly shown in the figure at frequencies of $\sim$0.0009 day^{-1} and 0.0018 day^{-1}, corresponding to characteristic periods of $P_1 \sim 1111$ days and $P_2 \sim 556$ days respectively. There is also a semi-persistent signal at frequency of 0.0037 day^{-1} corresponding to a periodicity of $P_3 \sim 270$ days. The three characteristic periods are comparable with those detected

in the LS periodogram and the Jurkevich method. However, periodic variations of P_3 are only present between JDs $\sim$ 2453750 and 2456450 and the WWZ power is much weaker than those of P_1 and P_2, as indicated in the lower panel of Figure 4. This explains why this signal has weak signatures in both the LS periodogram and Jurkevich plots. As for P_1, the frequency of the WWZ power has a decreasing trend in the time domain (from 0.00092 to 0.00082 day^{-1}). On the contrary, the WWZ power of P_2 is the strongest and the most stable, suggesting it is the most robust periodic signal in the present data set.

In order to evaluate the red noise effect on the WWZ results, we computed the time averaged WWZ power spectrum and constructed the curves of 2σ and 3σ confidence levels using the same procedures as in the LS periodogram. The result is displayed in the lower panel of Figure 4. The WWZ power spectrum features similar results as in the LS periodogram. The most prominent period is $P_2 = 541 \pm 42$ days. The uncertainty in the period is evaluated by the FWHM of a Gaussian fit of the corresponding peak. The peak of this period is well above the 3σ confidence level, once again demonstrating this period is intrinsic in the optical variations of 1ES 1959+650. On the other hand, the periodicities of $P_1 = 1124 \pm 216$ days and $P_3 = 268 \pm 19$ days only have significance levels of $>2\sigma$.

4. Physical Models

We have identified three possible periods in the optical light curve of 1ES 1959+650 using three different methods. There is a candidate period of $\sim$268 days (0.73 yr) with significance of $>3\sigma$ present in the LS periodogram. However, the Jurkevich results indicate that this periodic signal is very weak (with $f = 0.2$). In addition, the WWZ results show that this periodic variation is more like a transient phenomenon (only present between JDs $\sim$2453750 and 2456450). This is probably due to the observation data out of this time range being relatively sparse (see Figure 1), and some outburst peaks associated with this periodic variation may be missed. The Jurkevich method also reveals a significant period ($>3\sigma$) of $\sim$1100 days (3 yr), while this period is less significantly (only $>2\sigma$) detected by the other two methods. Besides, the total observation range of the data sample we used is merely $\sim$5 times this period. Thus, we cannot confirm these two periods based on the present data.

On the other hand, all three methods have revealed a confident periodicity of $\sim$540 days (1.48 yr) with significance of $>3\sigma$. Year-like periodic variations have been detected in a large number of blazars (see e.g., Zhang et al. 2014; Li et al. 2015; Sandrinelli et al. 2016 and references therein). Since 1ES 1959+650 is a blazar, any mechanisms that cause periodic variations should be correlated with the relativistic jet or the processes feeding the jet. Thus we classified the physical mechanisms into two groups and discussed their possibilities for the periodic variations detected in 1ES 1959+650.

4.1. Jet Model

Helical motion of the emitting materials in a twisted jet or jet precession could lead to a periodic change of the viewing angle of the jet. The resulting variability of the Doppler boosting then may cause a net apparent periodicity without changes in the intrinsic emission fluxes. These mechanisms are the so-called geometry models (Rieger 2004). Villata & Raiteri (1999) proposed that in a helical jet the emitting materials with higher emission frequencies may be located in a more twisted region and closer to the central engine than those with lower frequencies. This model has been used to explain the broad band SED variations of several blazars (see, e.g., Raiteri et al. 2017, 2021). However, helical motion caused by jet internal rotation generally has an observed period of $P_{\rm obs} \leqslant 10$ days for massive quasars (Rieger 2004), and thus it cannot be a plausible model for the case studied here. On the other hand, in a supermassive black hole (SMBH) binary system, the observed periods will be much longer ($P_{\rm obs} > 10$ days; Rieger 2004). This may explain the periodicity of 1.48 yr detected in 1ES 1959+650.

Alternatively, jet precession may also periodically change the viewing angle and generate periodic variability in blazars. Three-dimensional relativistic magnetohydrodynamic (MHD) simulations show that a tilted precessing disk can launch a relativistic jet that precesses together with the disk (Liska et al. 2018). Sobacchi et al. (2017) proposed a precessing jet model with corkscrew structures on the scale of a few parsecs to explain the few-year periodic variations in blazars. However, jet precession in a single SMBH system cannot account for periodicities with timescales less than several tens of years (Rieger 2004). Indeed, as discussed in Graham et al. (2015), the precession period would be between $10^{2.2}$ and $10^{6.9}$ yr for a typical quasar with SMBH mass of 10^8 $M_\odot$ and the absolute magnitude in the B band of $M_{\rm abs} = -25$. Shorter periods can be produced in an SMBH binary system. In this case, tidal interaction of a secondary SMBH will induce jet precession with periods of $P > 1$ yr (Rieger 2004). This timescale is also comparable with the periodicity detected in 1ES 1959+650.

Optical polarimetric observations of 1ES 1959+650 show a maximum variation of $\Delta\delta = 2.9$ for the Doppler boosting factor, with $\Delta\phi = 0.^\circ43$ for the viewing angle of the jet (Sorcia et al. 2013). This provides probable evidence for the geometrical models. However, the Very Long Baseline Array (VLBA) images of 1ES 1959+650 show a fairly straight jet structure on parsec scales (Rezzolla et al. 2003; Piner et al. 2010), making the situation very complicated.

4.2. Variations in Accretion Process

Periodic accretion oscillations can be excited near the inner edge of the accretion disk under the condition of $\alpha \gtrsim 0.1$ for a standard thin α-disk (Honma et al. 1992), and QPOs will be observed if these periodic oscillations propagate into the jet and

the observed brightness of the source. Relativistic MHD simulations show that magnetically choked accretion flows (MCAFs) will lead to jet-disk high-frequency quasi-periodic oscillations (HFQPOs) (Tchekhovskoy et al. 2011; McKinney et al. 2012). However, the oscillation periods are quite short, $\lesssim$1 day for a massive quasar (10^8 $M_\odot$) (Honma et al. 1992; McKinney et al. 2012). Alternatively, radiation pressure in the inner disk of high Eddington ratio black hole systems would break the accretion flow into rings with high and low surface densities (Lightman & Eardley 1974). If these rings were formed via thermal processes, the timescale would be ∼0.2 yr (King et al. 2013), which is also much shorter than the periodicity detected in the present work.

On the other hand, King et al. (2013) proposed that radio QPOs in FSRQ J1359+4011 are an analog of the low-frequency quasi-periodic oscillations (LFQPOs) seen in microquasars. LFQPOs in microquasars may be generated by dynamo cycles (O'Neill et al. 2011) or Lense-Thirring precession of a geometrically thick accretion flow (King et al. 2013). Simulations indicate that dynamo cycles have periods of ∼30 days for a massive black hole (10^8 $M_\odot$) (King et al. 2013), making it improbable to be a plausible mechanism for the periodic variation observed in 1ES 1959+650. However accretion flow precession would change the jet direction and lead to the observed periodic oscillations (King et al. 2013). For a typical microquasar with mass of 10 $M_\odot$ and exhibiting QPOs at 1 Hz, the analogous periodicity for 1ES 1959+650 (with mass of 1.5×10^8 $M_\odot$) would be ∼173 days. This is comparable to the periodicity detected here.

Global p-mode oscillations in a torus or a thick disk with finite radial extent can excite long-term quasi-periodic accretion (Rector et al. 2003; Liu et al. 2006; Wang et al. 2014). The oscillation frequencies are in the harmonic relationship 1:2:3:4:...:m, where m is an integer (Liu et al. 2006). It is interesting that we found possible multiple periods (0.73, 1.48 and 3 yr) in the optical data of 1ES 1959+650, although the two (0.73 and 3 yr) periods have relatively low significance. The frequencies of the three candidate periods show a relationship of 4:2:1. If this is the physical reason for the periodic variations in 1ES 1959+650, it will need some additional periods in the observed data. However, with the present data, we only detected three possible periodicities.

In an SMBH binary system with mass ratio $q > 0.1$, the binary torques would open a cavity in the inner portion of the circumbinary accretion disk (CAD) (MacFadyen & Milosavljevic 2008; Noble et al. 2012; Roedig et al. 2012). An overdense lump would be created in the inner edge of the CAD (Shi et al. 2012; Farris et al. 2014; D'Orazio et al. 2016), and periodically modify the accretion flux into the cavity and hence onto the mini-disks around each black hole (Farris et al. 2014; Bowen et al. 2018, 2019). This may cause multiple periodic variations in the observed flux in blazars. Significant periodicity in the total accretion rate were found in a periodogram at the binary orbital periods $t_{\rm bin}$ and ∼0.5 $t_{\rm bin}$ (D'Orazio et al. 2013, 2015; Farris et al. 2014). These periods can be interpreted as replenishment of the accretion flow of each black hole passing near the overdense lump (Farris et al. 2014). For $q \gtrsim 0.43$, besides the above two periods, there are also peaks of associated harmonics shown in the periodogram (Farris et al. 2014). If all of the three candidate periods are genuine, the periodic variations in the optical data of 1ES 1959+650 can be interpreted by this model, in which the two periods 1.48 and 0.73 yr correspond to the binary orbital and the half binary orbital periods, and the 3 yr period can be the associated harmonic. However, the two (0.73 and 3 yr) periods are severely affected by noises in the data, and thus more observations are required to identify this mechanism.

5. Conclusions

We analyzed the optical R band variations of the TeV blazar 1ES 1959+650 to search for QPOs in this object. The light curve spans a time interval of 15.6 yr. Three techniques were used to identify periodicities in the optical data. The LS periodogram revealed a strong periodicity of 540 ± 38 days. After accounting for the red noise processes, we found the significance level of this periodicity $>3\sigma$. Moreover, the Jurkevich method also detected a periodic oscillation with the same value of 540 ± 35 days in the data. This period is also statistically significant ($>3\sigma$), as estimated using the same model power spectrum as in the LS periodogram. We also adopted the WWZ method to identify the possible variation of this periodicity in the time domain, and it turns out that the period is quite persistent and stable through the whole observation interval. The time averaged WWZ power spectrum also reveals a peak at 541 ± 42 days with a confidence level of $>3\sigma$. All these results indicate that an intrinsic periodic oscillation with a period of ∼540 days exists in the optical variations of 1ES 1959+650.

Several physical models were proposed to explain the detected periodicity. Although the geometrical models (helical motion or jet precession) in an SMBH binary system are available to explain the year-like periodic variation in 1ES 1959+650, VLBA observations are opposite to the fundamental hypothesis of these models, that the relativistic jet is twisted in a helical or corkscrew pattern. Alternatively, periodic accretion oscillations may induce periodic variation in the observed brightness of this object. The period could be the analog of LFQPOs observed in microquasars. In addition, orbital motion of an SMBH binary system surrounded by a CAD could also be a possible mechanism for periodic oscillations in 1ES 1959+650. In order to identify the physical process, more observations are required for this object.

Acknowledgments

We gratefully acknowledge the anonymous referee for the helpful suggestions that improved this manuscript. Our research is supported by National Natural Science Foundation of China (Grant No. U1931106), Shandong Provincial Natural Science Foundation of China (Grant No. ZR2019YQ03) and Project of Shandong QingChuang Science and Technology Plan (Grant No. 2019KJJ006).

References

Abdo, A. A., Ackermann, M., & Ajello, M. 2010, ApJ, 710, 1271
An, T., Baan, W. A., Wang, J. Y., et al. 2013, MNRAS, 434, 3487
Anjum, M. S., Chen, L., & Gu, M. 2020, ApJ, 898, 48
Beaklini, P. P. B., & Abraham, Z. 2014, MNRAS, 437, 489
Bhatta, G., Stawarz, Ł., Ostrowski, M., et al. 2016, ApJ, 831, 92B
Bonning, E., Urry, C. M., Bailyn, C., et al. 2012, ApJ, 756, 13
Böttcher, M. 2005, ApJ, 621, 176
Böttcher, M. 2007, ASPC, 373, 169
Bowen, D. B., Mewes, V., Campanelli, M., et al. 2018, ApJ, 853L, 17B
Bowen, D. B., Mewes, V., Noble, S. C., et al. 2019, ApJ, 879, 76
Caproni, A., Abraham, Z., & Monteiro, H. 2013, MNRAS, 428, 280
Dai, Y., Wu, J., Zhu, Z. H., et al. 2013, ApJS, 204, 22
D'Orazio, D. J., Haiman, Z., Duffell, P., et al. 2015, MNRAS, 452, 2540
D'Orazio, D. J., Haiman, Z., Duffell, P., et al. 2016, MNRAS, 459, 2379
D'Orazio, D. J., Haiman, Z., & MacFadyen, A. 2013, MNRAS, 436, 2997
Espaillat, C., Bregman, J., Hughes, P., et al. 2008, ApJ, 679, 182
Fan, J. H. 2005, A&A, 436, 799
Fan, J. H., Liu, Y., & Yuan, Y. H. 2007, A&A, 462, 547
Fan, J. H., Xie, G. Z., Lin, R. G., et al. 1997, A&AS, 125, 525
Farris, B. D., Duffell, P., MacFadyen, A. I., et al. 2014, ApJ, 783, 134
Finke, J. D., Dermer, C. D., & Böttcherr, M. 2008, ApJ, 686, 181
Foster, G. 1996, AJ, 112, 1709
Gaur, H., Gupta, A. C., Strigachev, A., et al. 2012, MNRAS, 420, 3147
Giebels, B., Bloom, E. D., Focke, W., et al. 2002, ApJ, 571, 763
Graham, M. J., Djorgovski, S. G., Stern, D., et al. 2015, Natur, 518, 74
Gupta, A. C., Agarwal, A., Bhagwan, J., et al. 2016, MNRAS, 458, 1127G
Honma, F., Matsumoto, R., & Kato, S. 1992, PASJ, 44, 529
Jurkevich, I. 1971, Ap&SS, 13, 154
Kapanadze, B., Dorner, D., Vercellone, S., et al. 2018, ApJS, 238, 13
Kapanadze, B., Romano, P., Vercellone, S., et al. 2016, MNRAS, 457, 704
Kidger, M., Takalo, L., & Sillanpaa, A. 1992, A&A, 264, 32
King, O. G., Hovatta, T., & Max-Moerbeck, W. 2013, MNRAS, 436, 114
Krawczynski, H. 2004, NewAR, 48, 367
Krawczynski, H., Hughes, S. B., Horan, D., et al. 2004, ApJ, 601, 151
Kudryavtseva, N. A., Britzen, S., Witzel, A., et al. 2011, A&A, 526, 51
Kurtanidze, O. M., Tetradze, S. D., Richter, G. M., et al. 2009, ASPC, 408, 266
Li, H. Z., Chen, L. E., Yi, T. F., et al. 2015, PASP, 127, 1
Li, X. P., Luo, Y. H., Yan, H. Y., et al. 2017, ApJ, 847, 8
Lightman, A. P., & Eardley, D. M. 1974, ApJ, 187, 1
Liska, M., Hesp, C., Tchekhovskoy, A., et al. 2018, MNRAS, 474, 81
Liu, F. K., Zhao, G., & Wu, X. B. 2006, ApJ, 650, 749
Lomb, N. R. 1976, Ap&SS, 39, 447
MacFadyen, A. I., & Milosavljevic, M. 2008, ApJ, 672, 83
McKinney, J. C., Tchekhovskoy, A., & Blandford, R. D. 2012, MNRAS, 423, 3083
Meng, N. K., Zhang, X. Y., Wu, J. H., et al. 2018, ApJS, 237, 30
Nilsson, K., Lindfors, E., Takalo, L. O., et al. 2018, A&A, 620, 185
Noble, S. C., Mundim, B. C., Nakano, H., et al. 2012, ApJ, 755, 51
O'Neill, S. M., Reynolds, C. S., Miller, M. C., et al. 2011, ApJ, 736, 107
Perlman, E. S., Stocke, J. T., Schachter, J. F., et al. 1996, ApJS, 104, 251
Piner, B. G., Pant, N., & Edwards, P. G. 2010, ApJ, 723, 1150
Raiteri, C. M., Villata, M., Acosta-Pulido, J. A., et al. 2017, Natur, 552, 374
Raiteri, C. M., Villata, M., Larionov, V. M., et al. 2021, MNRAS, 504, 5629
Rani, B., Gupta, A. C., Joshi, U. C., et al. 2010, ApJ, 719, L153
Rector, T. A., Gabuzda, D. C., & Stocke, J. T. 2003, AJ, 125, 1060
Ren, G. W., Zhang, H. J., Zhang, X., et al. 2021, RAA, 21, 75
Reynoso, M. M., Medina, M. C., & Romero, G. E. 2011, A&A, 531, 30
Rezzolla, L., Yoshida, S., & Zanotti, O. 2003, MNRAS, 344, 978
Rieger, F. M. 2004, ApJ, 615, 5
Roedig, C., Sesana, A., Dotti, M., et al. 2012, A&A, 545, 127
Sandrinelli, A., Covino, S., Dotti, M., et al. 2016, AJ, 151, 54
Scargle, J. D. 1982, ApJ, 263, 835
Shi, J. M., Krolik, J. H., Lubow, S. H., et al. 2012, ApJ, 749, 118
Sobacchi, E., Sormani, M. C., & Stamerra, A. 2017, MNRAS, 465, 161
Sorcia, M., Benítez, E., & Hiriart, D. 2013, ApJS, 206, 11
Tchekhovskoy, A., Narayan, R., & McKinney, J. C. 2011, MNRAS, 418, 79
Timmer, J., & Koenig, M. 1995, A&A, 300, 707
Urry, C. M., & Padovani, P. 1995, PASP, 107, 803
Uttley, P., McHardy, I. M., & Papadakis, I. E. 2002, MNRAS, 332, 231
VanderPlas, J. T. 2018, ApJS, 236, 16
Vaughan, S. 2005, A&A, 431, 391
Vaughan, S., Uttley, P., Markowitz, A. G., et al. 2016, MNRAS, 461, 3145
Villata, M., & Raiteri, C. M. 1999, A&A, 347, 30
Wang, J. Y., An, T., Baan, W. A., et al. 2014, MNRAS, 443, 58
Xie, G. Z., Yi, T. F., Li, H. Z., et al. 2008, AJ, 135, 2212
Yuan, Y. H., Fan, J. H., & Pan, H. J. 2015, ApJ, 150, 67
Zhang, B. K., Zhao, X. Y., Wang, C. X., et al. 2014, RAA, 14, 933
Zhang, Y. H., & Li, J. C. 2017, MNRAS, 469, 1682